Very Small Bubble Formation at the Solid−Water Interface

Jingwu Yang, Jinming Duan, Daniel Fornasiero, and John Ralston*

Ian Wark Research Institute, University of South Australia, Mawson Lakes Campus, Mawson Lakes, Adelaide, SA 5095, Australia

Received: November 12, 2002; In Final Form: March 3, 2003

The formation of very small gas bubbles (so-called "nanobubbles") at structured solid−water interfaces has been studied using the tapping mode atomic force microscopy (TMAFM) imaging technique. Silicon oxide wafer surfaces were prepared with different degrees of nanometer scale surface roughness and hydrophobicity. Small bubbles do not form on smooth, hydrophilic, or dehydroxylated silicon oxide wafer surfaces immersed in aqueous solutions under known levels of gas supersaturation. Randomly distributed small bubbles were observed over the whole surface of observation on methylated surfaces of controlled roughness. Bubbles formed on rough, methylated surfaces were larger and less-densely distributed than those on a smooth surface of similar hydrophobicity. The process of bubble coalescence was observed as a function of time. The macroscopic contact angle, measured with respect to the aqueous or gas phase, is very different from the microscopic contact angle detected by TMAFM and appears to be due to the influence of line tension at the pinned three-phase contact line. The latter has a value of -3×10^{-10} N and acts to stabilize the small bubbles, flattening them and thereby reducing the Laplace pressure.

Introduction

Bubble formation at the solid−water interface is a topic of fundamental interest accompanied by significant commercial applications.[1,2] It is known that bubble formation on a solid surface immersed in water is certainly dependent on surface heterogeneities, as well as gas supersaturation.[3−7] Surface roughness and hydrophobicity affect bubble nucleation or formation or both and have been studied for decades.[7−10] From the classical point of view of bubble nucleation, preexisting gas cavities or Harvey nuclei[3] play an important role in bubble formation. Once gas cavities exist on a substrate surface, bubble formation can proceed at fairly low levels of gas supersaturation.[2]

Gas cavity formation on solid surfaces has been related to physical "defect points", normally termed "grooves" or "crevices" on solid surfaces. Generally, the formation of bubbles on these surface sites (which we now use as a generic description) depends on the geometry and size, as well as the wetting properties.[5,11] In bubble nucleation, gas may first be trapped at surface sites on a solid surface; further diffusion of dissolved gas from bulk solution would then enhance bubble formation,[11] a process related to the solid surface hydrophobicity,[12] as well as the level of gas supersaturation.

From a purely theoretical standpoint, the probability of bubble formation should be enhanced for water adjacent to a hydrophobic surface. The structure of water molecules next to a hydrophobic surface is apparently less ordered than that of the bulk phase,[13,14] while the cohesive strength of water may be significantly reduced at a water−hydrophobic solid interface.[15] However, experimental evidence to date suggests that the effect of surface hydrophobicity on bubble nucleation is evident only for *rough* hydrophobic solid surfaces,[7,9] where submicrometer gas bubbles congregate.[10,16,17]

Despite this previous research, the mechanism of bubble formation is still not clear. For example, the "critical size" of surface physical defects or crevices necessary for bubble formation has never been defined; rather bubble formation has been examined generally through the observation of large, or at least optically detectable, gas bubbles. Little experimental evidence has been obtained for nano or submicrometer bubble formation at solid−water interfaces. Examination of nano or submicrometer bubble formation on well-defined surfaces should provide useful information concerning bubble nucleation.

Recently, with the advent of tapping mode atomic force microscopy (TMAFM), imaging of nano or submicrometer bubbles formed on solid surface has become of interest in colloid science.[18−20] This research was spurred by a desire to explain the nature of the long-range hydrophobic forces often observed between hydrophobic solid surfaces immersed in aqueous solutions.[21−27]

The TMAFM technique can "image" very small bubbles on solid substrate surfaces because it has the capacity to determine both the physical structure and physicochemical nature of soft and fragile surfaces at the molecular level, provided that these surfaces are stable during scanning.[28,29] To date, the results of the TMAFM imaging of very small bubbles have yielded quite diverse results for "nanobubble" formation at solid−water interfaces.[18−20] Lou et al.[18] showed that small bubbles less than 100 nm in diameter could form on both hydrophobic (highly oriented pyrolytic graphite) and hydrophilic (freshly cleaved mica) surfaces. Using silicon wafers substrates modified by octadecyltrichlorosilane (OTS; root-mean-square (rms) roughness < 0.2 nm; θ_w, water-advancing contact angle, of 110°), Ishida et al.[19] observed that small bubbles with a base diameter of 650 nm and a height of 40 nm were *linearly* distributed on the substrate surface of observation. Accompanying force measurements by AFM suggested the existence of a long-range hydrophobic force between surfaces with bubble domains. Recently, TMAFM imaging by Tyrrell and Attard[20] showed

* To whom correspondence should be addressed. E-mail: john.ralston@unisa.edu.au.

10.1021/jp0224113 CCC: $25.00
Published on Web 05/30/2003

domains that were very different from those observed by Ishida et al.[19] The domains cover the whole hydrophobized surface of the substrate (methylated by dichlorodimethylsilane vapor; rms roughness < 0.5 nm; $\theta_{water,advancing} = 101°$, $\theta_{water,receding} = 80°$, hysteresis of 21°). The domains had a mean height of 20−30 nm and mean diameter of 71−87 nm. Because the surface roughness of the substrate surfaces used[19,20] in these two studies is rather similar, the differences in behavior are not readily explained.

The objectives of this study are to investigate the formation of very small bubbles at solid−water interfaces through TMAFM imaging of well-defined substrate surfaces with known degrees of surface roughness, hydrophobicity, and gas supersaturation. We demonstrate that there is a significant difference between the macroscopic contact angle for these substrates and the microscopic angle when a very small bubble is formed. The origin of this difference may be due to the line tension acting at the solid−water−vapor contact line.

Experimental Section

Reagents. Trimethylchlorosilane (TMCS, redistilled, 99+%) was obtained from Aldrich and was stored in a vacuum desiccator over phosphorus pentoxide (P_2O_5, A. R.). Cyclohexane (A. R., 99%) was obtained from Chem-Supply, South Australia. TMCS solutions in cyclohexane were freshly prepared in 100 cm^3 standard flasks under an atmosphere of high-purity nitrogen (>99%).

High-purity Milli-Q water was supplied by an Elga UHQ water system with a conductivity less than 1×10^{-6} S cm^{-1}, surface tension of 72.8 mN m^{-1}, and pH = 5.6 at 20 °C. Water saturated with CO_2 was equilibrated at elevated pressures using high-purity CO_2 (food grade) in a pressure chamber for 30 min, which reduced the pH to 4.2 (see later).

All other chemicals were of analytical grade and were used as received.

Oxidized Si(100) wafers (one-side polished, Philips, Eindhoven, Netherlands) were used as substrates. The rms roughness of the silicon wafers was less than 0.1 nm, while the maximum peak to trough distance was approximately 0.3 nm over an area of 1×1 μm^2.

Surface Cleaning. Clean wafer substrates were prepared according to the following steps: (1) substrates were subjected to sonication in ethanol and cyclohexane for 30 s and then rinsing with Milli-Q water and treatment in an air plasma (Harrick Plasma Cleaner/Sterilizer PDC-32) for at least 30 s; (2) the substrates were then placed in a bath of H_2SO_4 (98%)/H_2O_2 (30%) (3:1 in volume) at 80 °C for 30 min, generously rinsed with Milli-Q water, and bathed in hot Milli-Q water for 30 min; (3) substrates were dried in a stream of N_2 (N_2 was passed through a filter with pore size of 50 nm before it passed into the glovebag so as to remove any possible particles), then stored in a glass reaction vessel, and finally dried in a clean oven at 120°C for 2−3 h; (4) the substrates were sealed in a clean container prior to surface modification (see below). This process was performed prior to surface modification to minimize any contamination.

Surface Modification. *Dehydroxylated Surfaces.* Substrates were heated at 1050 °C in a clean oven overnight and allowed to cool in air. At this temperature, substantial dehydroxylation[30,49] occurs at the oxidized silicon wafer surface, resulting in an advancing water contact angle of about 42°.

Methylation with TMCS Vapor. The clean substrates were transferred to a glovebag filled with nitrogen and then immediately placed inside a sealed bottle containing a small beaker filled with 5 cm^3 of pure TMCS liquid and left for 20 min. After methylation, the substrates were rinsed with cyclohexane again to remove residual silane and then dried in a clean room at room temperature.[31]

Methylation with TMCS Solution. The substrates in the sealed glass vessel were first transferred to a glovebag from the oven (see surface cleaning) while a continuous N_2 gas supply to the bag was maintained; 40 cm^3 of 2×10^{-4} M TMCS solution was then rapidly transferred to the reaction vessel in the bag. Using this process, one prevents the reaction of TMCS with water vapor in the air. After a measured reaction time, the substrate was rinsed thoroughly with cyclohexane several times in the glovebag and then dried with high-purity nitrogen in a clean room at room temperature. An exposure time of 20 min was used to produce a rough and hydrophobic surface.

The water-advancing and -receding contact angles of the prepared substrates were measured by using the sessile-drop method to compare the surface hydrophobicity and assess the degree of hysteresis.[32]

TMAFM Imaging. Unlike AFM contact mode imaging, in TMAFM, the cantilever is vibrated at or near its resonant frequency; the tip gently taps the surface and then lifts off vertically so that it can protect both the sample and the tip from "damaging" during scanning.[33] In TMAFM scanning, topography and phase shift images can be collected at the same time. It is known that the phase image in TMAFM is more sensitive for detecting variations in material properties such as adhesion and viscoelasticity. This enables TMAFM to image very small and similar soft matter such as very small bubbles on solid surfaces.[34]

TMAFM imaging for very small bubble observation was performed with a Nanoscope III (Digital Instruments), using a tapping mode fluid cell supplied by the manufacturer. The TMAFM imaging in air was performed only when dry surface feature characterization was of interest. The resonance frequency and spring constant of ultrasharp, noncontact silicon cantilevers (Silicon-MDT Ltd. Company) in air were 265−400 kHz and 20−75 N/m, respectively. Imaging in aqueous solutions was performed using narrow, thin Si_3N_4 cantilevers (0.34 N/m, DI Inc) at frequencies in the range of 6.5−9.3 kHz. The cantilever surfaces were rinsed with ethanol and then cleaned in the plasma reactor for 30 s each time before use. All of the experiments were performed at 22 ± 2 °C in a class 100 clean room.

Two kinds of images were obtained simultaneously: height and phase images. The tapping strength can be controlled by the amplitude of the free oscillation (A_0) and the set-point amplitude (A_{sp}) of the cantilever. Normally, a suitable driving amplitude was selected to give a 0.5 V rms amplitude. It was found in this study that the selection of A_{sp} is critical to obtaining a high-quality image. However, the optimal A_{sp} is not a constant value but varies according to the substrate. Once the optimal A_{sp} was selected for an individual sample, it remained stable for several hours. Typically, the phase image was dominated by the mechanical properties of the substrate surfaces if a higher rms amplitude and lower A_{sp} were applied. A lower A_{sp} reflects a stronger interaction between the tip and substrate; thus a better indication of the surface features may be obtained. Hence, the A_{sp} must be selected so that it is small enough to "sense" the domains on the substrate surface yet not too low so as to damage the fragile surface features.

Phase imaging can be used as "compositional mapping" because it reflects differences in energy dissipation due to variations in adhesive, mechanical, and viscoelastic properties over heterogeneous surfaces, depending on tapping strength.[34]

If very small bubbles are detected on the silicon wafer surface, a significantly high phase shift (>25°) should be seen between a bubble and bare parts of a substrate surface.[19] A weak repulsive force between the hydrophilic tip and a gas bubble is essential for the TMAFM bubble imaging.[18,19,30]

All images were obtained using the "E" scanner with a scan rate of 1 Hz. For each separate experiment, at least three separate images were obtained. The images were found to be both stable and reproducible.

Dissolved CO_2 Control. CO_2 solutions were used in this study for the purposes of bubble formation and observation because (i) CO_2 is the most soluble "common" gas in water so a high supersaturation can be obtained easily without application of very high pressure and (ii) the CO_2 concentration can be easily and accurately determined simply by measuring the solution pH.[35] In all of the experiments, the Milli Q water (at pH 5.6) was supersaturated with CO_2 in a sealed pressure vessel so that the pH of the CO_2 water solution was 4.2, corresponding to a concentration of 0.01 M of gaseous, molecular CO_2. The preparation process is as follows: (1) 150 cm^3 of Milli-Q water was degassed under a vacuum pump for 30 min; (2) Milli-Q water was pressurized in a small bottle with pure CO_2 in a pressure chamber at 2 atm for 30 min (CO_2 was allowed to pass through the chamber to purge the air for a few minutes before the vessel was closed; stirring was applied during saturation); (3) the chamber pressure was released; solution pH normally was measured at around 3.9; (4) the bottle was sealed and shaken for a few minutes; (5) the bottle was opened to air and the pH measured immediately; (6) steps 4 and 5 were repeated until the pH was 4.2. The resulting solution was optically clear with a dissymmetry ratio of 1.00 at 430 nm.

This dissolved CO_2 in Milli-Q water solution was used for the purpose of surface bubble nucleation. It was first injected into the AFM fluid cell (with the substrate to be scanned inside), and then the cell was flushed with Milli-Q water for several times before TMAFM imaging. This flush with Milli-Q water was designed to yield a high level of gas supersaturation with respect to CO_2 in the water layer adjacent to the prepared substrate surfaces, which is favorable for bubble nucleation. By this method, very small bubbles that formed at the solid−water interface were imaged reproducibly.

Results

Substrate Surface Characterization in Air. The surface features of the solid substrates were characterized by TMAFM imaging in air, while the surface hydrophobicity was assessed by contact angle measurements using the sessile drop method. The physical surface features are clearly displayed by using a height scale of 5 nm, as well as by a cross section profile. The surface roughness was also expressed in terms of rms roughness and peak-to-valley height (PTV).

The TMAFM image(s) of a clean hydrophilic Si-wafer surface (Figure 1) showed the same surface morphological features as those discussed elsewhere.[36] The substrate surface is clean and smooth with a distinct morphology, rms roughness of 0.09 nm over a 1 μm × 1 μm area (Figure 1a), and a PTV distance around 0.3 nm (Figure 1b). The silicon wafer surface is of a surface quality comparable to freshly cleaved mica surface in terms of surface roughness. Contact angle measurements showed instant and spontaneous spreading of a drop of water over the whole surface, indicating a hydrophilic surface with a contact angle of zero.

In Figure 2, the TMAFM image of a dehydroxylated clean Si-wafer surface is shown. Although the surface morphology shows an observable alteration and the surface roughness increased slightly, compared with the original hydrophilic wafer

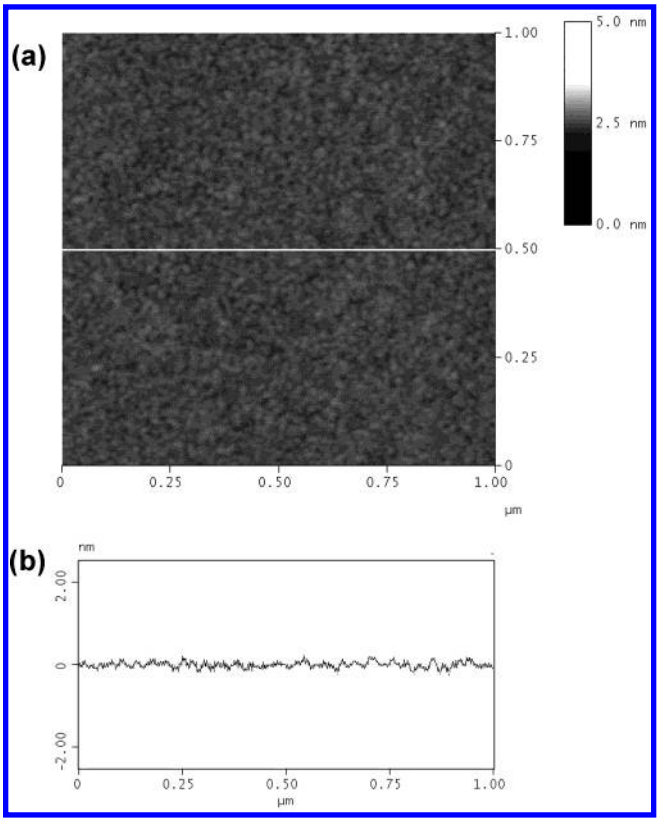

Figure 1. AFM tapping mode image (a) of clean Si surface and (b) height variation of cross section in air: image area = 1 μm × 1 μm; height = 5 nm.

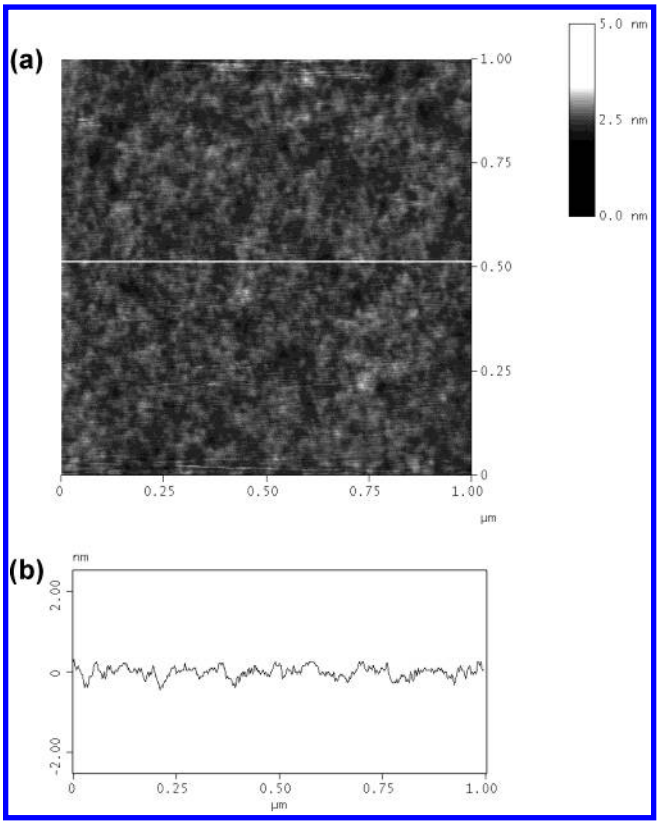

Figure 2. AFM tapping mode image (a) of dehydroxylated Si surface and (b) height variation of cross section in air: image area = 1 μm × 1 μm; height = 5 nm.

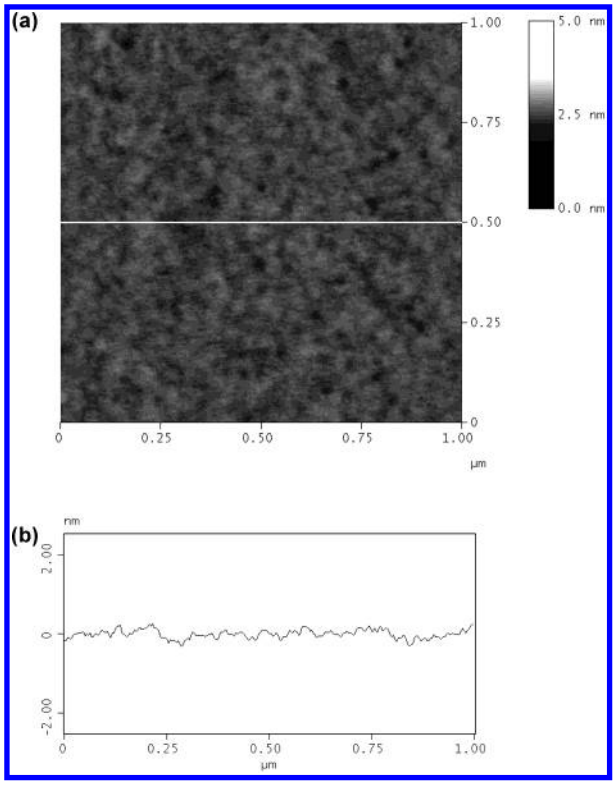

Figure 3. AFM tapping mode image (a) of Si surface modified with TMCS vapor for 20 min and (b) height variation of cross section in air: image area = 1 μm × 1 μm; height = 5 nm.

TABLE 1: Surface Roughness and Water Contact Angle for Clean and Hydrophobized Si-Wafers[a]

substrate surfaces	advancing contact angle	receding contact angle	rms roughness (nm)	PTV distance (nm)
clean Si-wafer	spreading		0.09	0.3
dehydroxylated (1050 °C)	42 (146)	34 (138)	0.2	0.5
exposed to TMCS vapor (20 min)	74 (113)	67 (106)	0.1	0.4
exposed to TMCS/cyclohexane solution (20 min)	88 (113)	67 (92)	2.7	12.3

[a] Air contact angles are given in parentheses. There was no detectable difference between air and carbon dioxide.

surface (see Figure 1), the overall surface roughness is still around the same magnitude (roughness = 0.2 nm; PTV distance = 0.5 nm). Some degree of "surface sintering" has apparently occurred during dehydroxylation.[49] The water-advancing contact angle (θ_w) of the dehydroxylated Si-wafer surface is 42°, as expected after the heating/dehydroxylation treatment.[30]

In Figure 3, the TMAFM image of a TMCS vapor methylated Si-wafer surface showed a distinct surface morphology compared with the original clean substrate. Surface "soft" and "larger" patterns were observed, in contrast to the "hard" and small "grainy" features of the clean Si-wafer surface (see Figure 1). The TMCS vapor methylation process resulted in very little alteration of the surface roughness of the clean wafer surface: the rms roughness was 0.1 nm, and PTV distance was 0.4 nm, similar to those of the original clean, untreated surface. The hydrophobicity of the methylated substrate is high (θ_w = 74°) with a small degree of hysteresis (see Table 1), in agreement with earlier observations.[22,31]

A TMAFM image of the TMCS/cyclohexane solution methylated Si-wafer surface is shown in Figure 4. In comparison

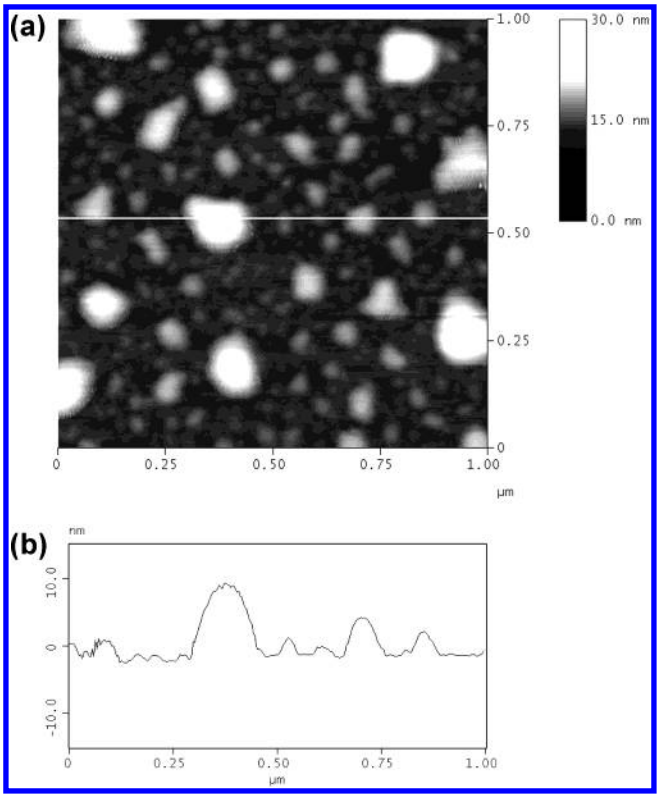

Figure 4. AFM tapping mode image (a) of Si surface modified with TMCS solution for 20 min and (b) height variation of cross section in air: image area = 1 μm × 1 μm; height = 30 nm.

with the TMCS vapor-treated surface, the TMCS/cyclohexane solution methylated wafer surface showed very different surface features with marked nanometer scale surface roughness: rms roughness = 2.7 nm; PTV distance = 12.3 nm, providing an ideal surface for examining surface roughness effects on bubble formation. This rough surface feature resulting from TMCS/cyclohexane solution treatment is believed to be due to the existence of trace quantities of water in the cyclohexane solvent (a few parts per million). Interaction of TMCS with this trace water can produce hydrolysis products, such as dimethyldisiloxane, which then deposit on the wafer surface, resulting in rough surface features.[37−39] The water-advancing contact angle was measured at 88°, substantially higher than that of TMCS vapor prepared Si-wafer surface and in accord with previous studies (e.g., refs 31 and 37).

A summary of the parameters for the surface features examined is given in Table 1. Note that for each condition at least five independent substrates were examined.

Imaging of Substrate Surfaces Immersed in CO_2 Saturated Aqueous Solutions. The various wafer substrate surfaces were examined by TMAFM when immersed in dissolved CO_2 Milli-Q water solution ($[CO_2]$ = 0.01 M). The results are given in the following.

Imaging of Clean Hydrophilic Si-Wafer Surfaces. A TMAFM image of hydrophilic Si-wafer substrates immersed in the CO_2 solution is shown in Figure 5. A smooth substrate surface is evident and is very similar to the image obtained in air (see Figure 1).

Note that the surface roughness and morphology shown in Figure 5 are slightly different from those shown in Figure 1. However, these minor differences are not due to any physical change of the substrate surface itself; rather, they are likely due to the effect of the medium on TMAFM imaging. Hydrodynamic or viscous effects or both can influence the vibration of the

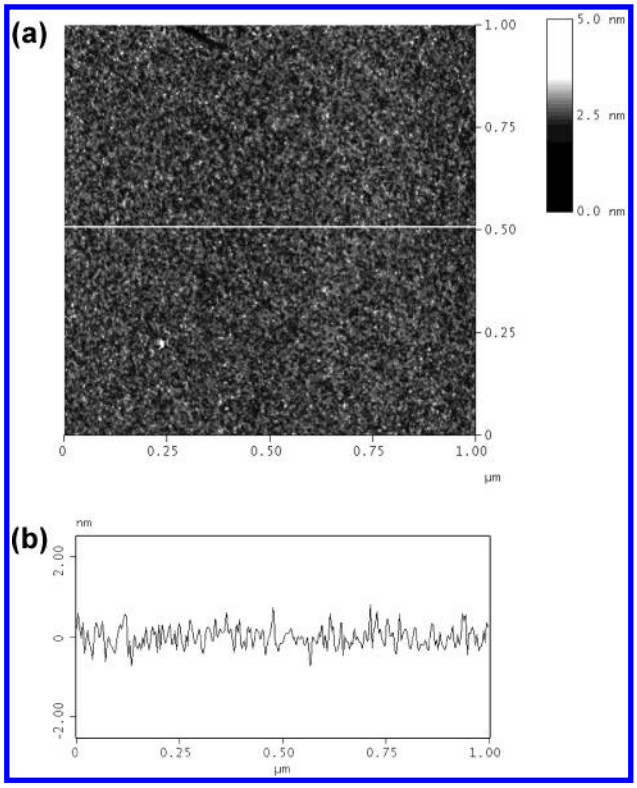

Figure 5. AFM tapping mode image (a) of clean Si surface and (b) height variation of cross section in saturated CO_2 solution: image area = 1 μm × 1 μm; height = 5 nm.

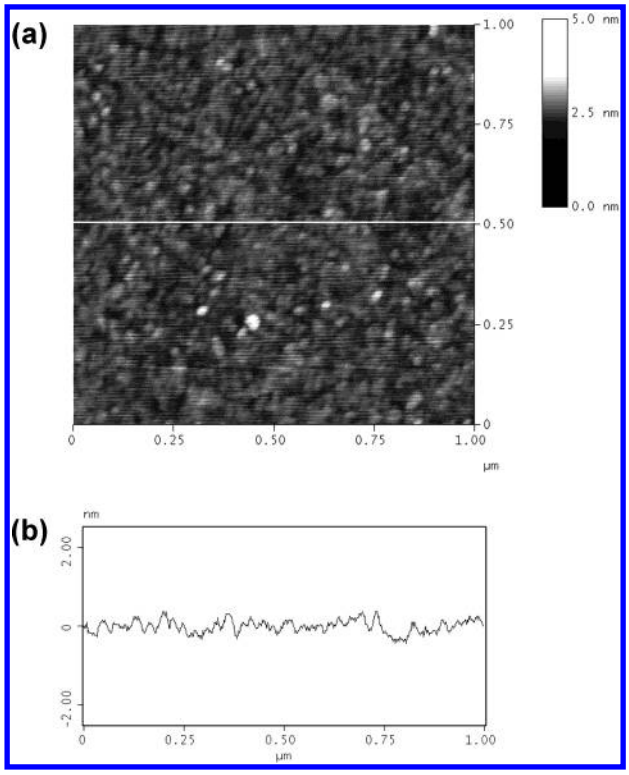

Figure 6. AFM tapping mode image (a) of dehydroxylated Si surface and (b) height variation of cross section in saturated CO_2 solution: image area = 1 μm × 1 μm; height = 5 nm.

cantilever in water, and in addition, modification of the interfacial forces between the cantilever and substrate surface in water may cause a slight difference in the TMAFM images obtained in air and aqueous solutions for the same substrates.[40]

Dehydroxylated Si-Wafer Surface. A TMAFM image for the dehydroxylated Si-wafer surface in CO_2-saturated solution is shown in Figure 6. As in the case of hydrophilic substrates, the image obtained showed smooth surface features (see Figure 6b), similar to those obtained in air (Figure 2). Slight morphological variations in comparison to those obtained in air were observed.[40] There was no evidence for bubble formation on the dehydroxylated wafer surface (with an intermediate hydrophobicity, $\theta_w = 42°$). This observation is consistent with the earlier observation that a clean, dehydroxylated silicon-wafer surface exhibits no sign of long-range attraction or long-range jump distances in the AFM force versus distance measurements between dehydroxylated silicon surfaces.[22] Moreover, we do not detect any influence of CO_2-saturated solutions on the coagulation stability of dehydroxylated silica particle dispersions.[53]

TMCS Vapor Prepared Si-wafer Surface. TMAFM height and phase images for TMCS vapor prepared Si-wafer surfaces are shown in Figures 7 and 8, respectively. In contrast to the smooth surface features obtained in air for the same kind of substrate surface (see Figure 3), clear domains cover quite randomly the whole surface of observation. If, for now, we assume that these domains are bubbles, the base radius and height of these bubbles are in the range between 50 and 400 nm and 20 and 80 nm, respectively. The size range of these bubbles and the manner of their distribution are similar to those observed by other researchers.[18,19] However, the bubbles shown in the image in Figure 7 are much more densely populated and much more evenly distributed over the whole surface of observation compared with those observed by Ishida et al.[19]

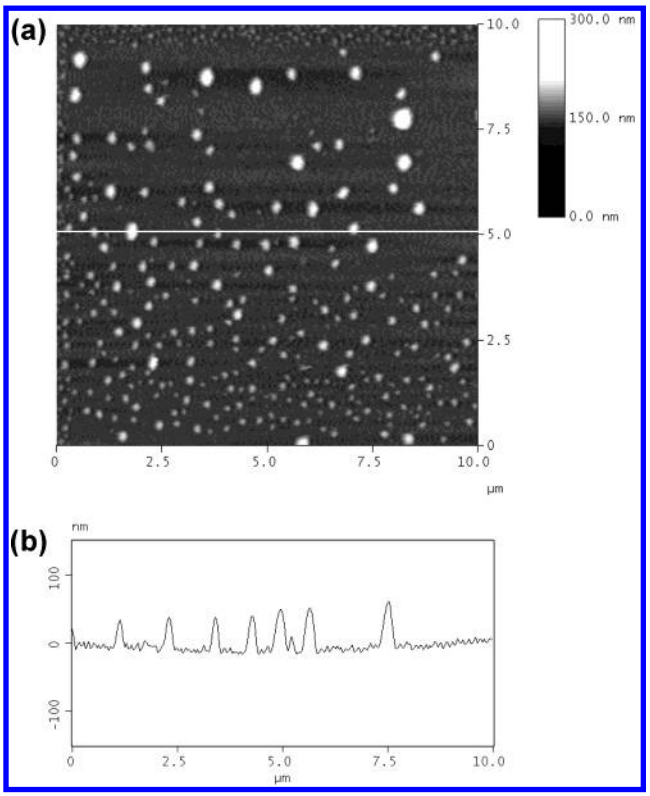

Figure 7. AFM tapping mode image (a) of Si surface modified with TMCS vapor for 20 min and (b) height variation of cross section in saturated CO_2 solution: image area = 10 μm × 10 μm; height = 300 nm.

TMCS/Cyclohexane Solution Prepared Si-Wafer Surface. The TMAFM image for the "rough" surface obtained by TMCS/cyclohexane solution methylation is shown in Figure 9. In comparison with the bubbles for the smooth surface (see Figure

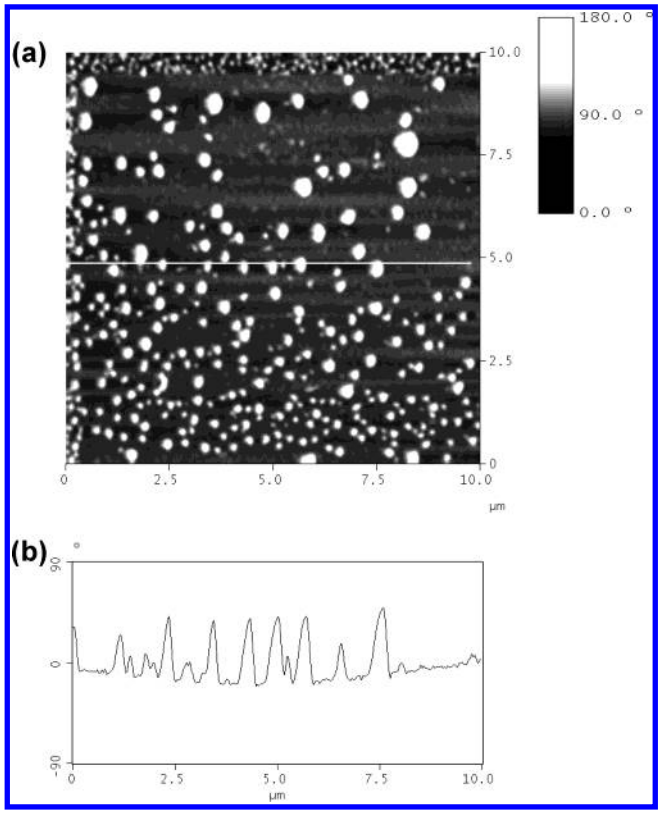

Figure 8. AFM tapping mode phase image (a) of Si surface modified with TMCS vapor for 20 min and (b) phase shift variation of cross section in saturated CO_2 solution: image area = 10 μm × 10 μm; phase shift = 180°.

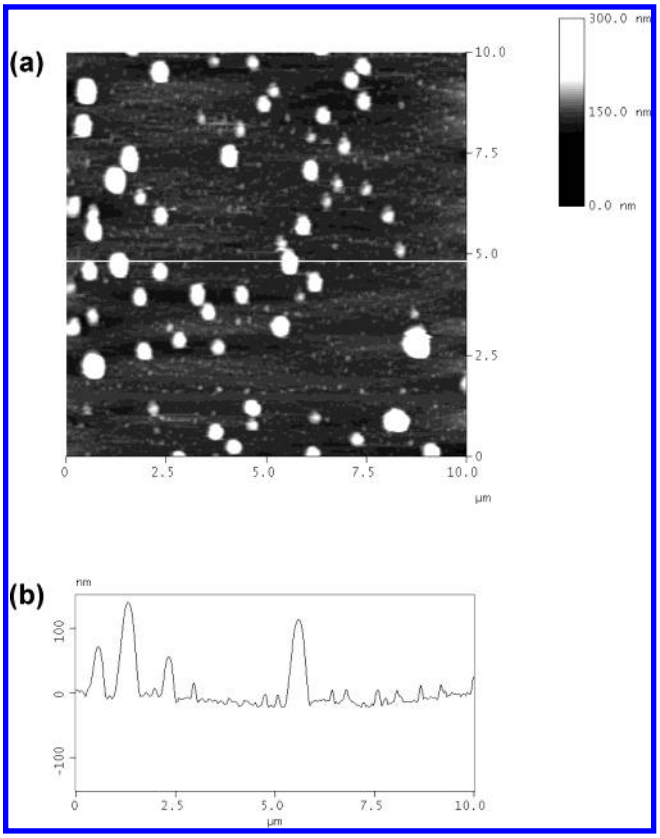

Figure 9. AFM tapping mode image (a) of Si surface modified with TMCS solution for 20 min and (b) height variation of cross section in saturated CO_2 solution: image area = 10 μm × 10 μm; height = 300 nm.

7), one major difference is that bubbles on the rough surface are much less densely populated and the bubble sizes are relatively larger than those for the smooth surface. The bubble base radius and height are around in the range of 150−400 nm and 60−200 nm, respectively. Note that a distinct surface pattern is reflected in the baselines in the cross section profile, evidenced by small individual peaks. These different features of bubble size and distribution reflect the effects of surface roughness on bubble formation. Note that the same degree of phase shift was observed over the domains as in the case of the TMCS vapor prepared substrate.

Images of Bubble Coalescence. Consecutive imaging by the TMAFM at time intervals over a long time scale was performed to provide further evidence as to the character of the domains observed by the TMAFM imaging. The substrates used were the TMCS/cyclohexane solution prepared Si-wafer (θ_w = 88°, rms roughness = 2.7 nm, see Table 1). The early stage of the TMAFM imaging process was the same as for normal imaging (Figure 9). However, after the completion of the first TMAFM image, the fluid cell was flushed gently using a 10 cm^3 syringe with Milli-Q water every 20 min, and the images were followed by TMAFM scanning. This whole process lasted for more than 20 h. The first image was similar to the bubble image shown in Figure 9; five sets of bubble images thereafter are presented in Figure 10a−e.

First, one can see in this series of images that, after long-time TMAFM scanning, the bubbles that initially distribute evenly over the whole surface "line up" around a vertical line in the observation area. This phenomenon seems to be evident in TMAFM images reported elsewhere, albeit indistinctly.[18,19] It can be reasonably assumed that such a pattern of behavior may be attributed to some fluid−bubble perturbation by the cantilever during the extended horizontal movement or scanning in the fluid cell. This perturbation may also contribute to bubble coalescence.

However, the single most important observation from these images is the process of bubble coalescence and the disappearance of an individual bubble from the solid−solution interface surface, behavior that is characteristic of gas bubbles in aqueous solutions. For example, the smaller bubble (in the broken line circle) becomes even smaller from image a to image d in Figure 10, and finally "dissolves" or merges with the neighboring bubble so that the latter becomes a larger bubble. An individual small bubble (identified by arrow) becomes increasingly smaller from image a to image c in Figure 10 and finally disappears from image d. The observed phenomenon, namely, that a smaller bubble becomes smaller or dissolves while the neighboring bigger bubble becomes larger, is quite similar to "Ostwald ripening".[41,42] It is the first time that such a very small bubble ripening or coalescence process has been observed by TMAFM imaging.

Discussion

Nature of Domains. Regarding the nature of the domains, several pieces of evidence identify them as gas bubbles: (1) The first important evidence is the large phase shift (approximately 50°) observed over the domains during phase imaging (see Figure 8). This large phase shift indicates that the domains are soft and different in nature from the hydrophobized solid surfaces.[34] A typical view of the phase shift across a bubble, generated from TMAFM data files, is shown in Figure 11. From this figure, one can see that, although the cross section of the bubble can be fitted to a spherical cap curve (note the

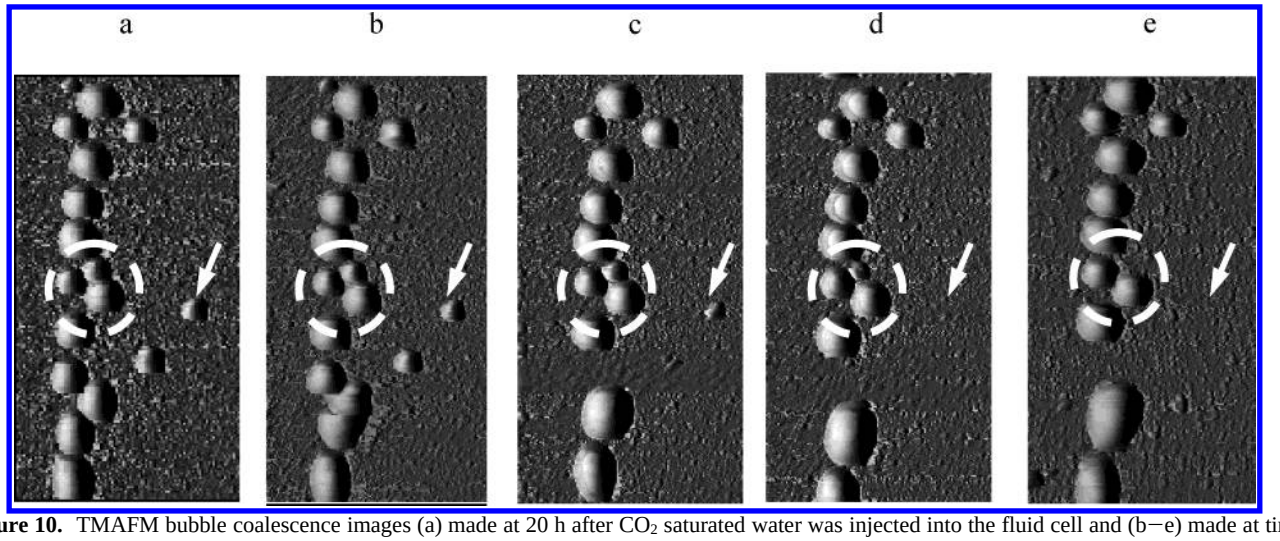

Figure 10. TMAFM bubble coalescence images (a) made at 20 h after CO_2 saturated water was injected into the fluid cell and (b−e) made at time intervals of 20 min after image a was taken: scan area = 10 μm × 5 μm; height = 300 nm.

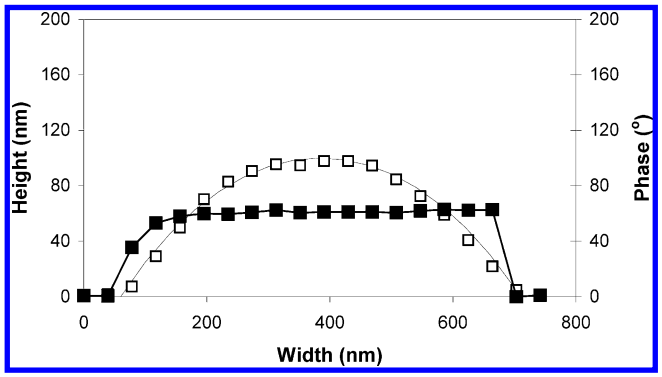

Figure 11. Cross section of a bubble height and phase image profile created from TMAFM image file (TMCS vapor treatment Si-wafer, supersaturated CO_2 solution): (□) height image; (■) phase image.

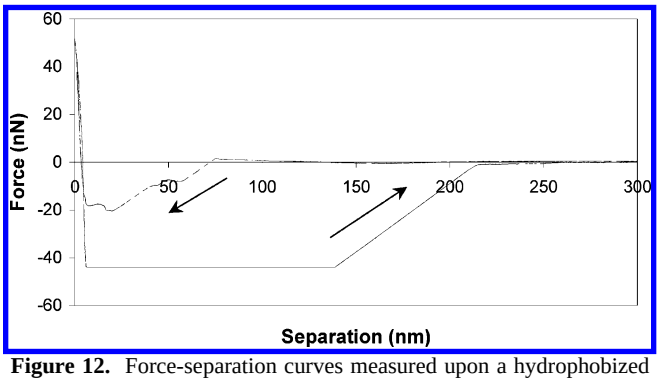

Figure 12. Force-separation curves measured upon a hydrophobized silica colloid probe approaching (broken line) and retreating from (solid line) a small bubble formed on a methylated Si-wafer surface.

different scales for the base and the height), a constant phase value of around 50° across virtually the whole distance of the selected bubble was seen. (2) Because TMCS, a small molecule (MW = 108.64), is attached through −Si−O−Si− bonds with the Si-wafer surface,[31,37,49] it is very unlikely that these adsorbed TMCS molecules, after vapor treatment of the solid surface, will accumulate into large domains on the substrate surface when it is immersed in the fluid cell. (3) The evidence for bubble coalescence or Ostwald ripening (see Figure 10) also supports very strongly that the domains are gas bubbles. These domains would only coalesce or dissolve if they are indeed gas bubbles; domains of polymeric material would not be expected to coalesce nor change in size over the time frame of observation. Furthermore, we note that in very strongly degassed solution the structures observed did not change with time and were little different from those shown in Figure 4. Their mechanical properties are different from bubbles. The force versus distance behavior is indicative of the presence of bubbles on the solid surface.[19,23,26]

The force measurements for a colloid probe approaching and then separating from the bubble-covered, solution-methylated Si wafer surface were obtained by using a methylated silica colloid probe (radius = 8 μm) (Figure 12). We have described the procedures elsewhere.[22,30] The long-range jump distance (>70 nm) for the approaching probe, coupled with the high adhesion force during retreat, is characteristic of the presence of gas bubbles on these surfaces.[19,22,26] The stepwise character of the force versus distance curve is consistent with bubble bridging for this rough surface.[23]

Bubble Formation on Solid−Water Interfaces. TMAFM images show that there is no nanobubble formation on smooth *hydrophilic* surfaces. This is in agreement with earlier observations in the literature[3,7,9,43] but in contrast to a recent report[18] that nanobubbles are present on freshly cleaved (hydrophilic) mica surfaces.

For dehydroxylated surfaces, there was no nanobubble formation. Bubble formation does not occur on this smooth surface with intermediate hydrophobicity (θ_w = 42°) and a small degree of hysteresis (see Table 1).

However, when the surface hydrophobicity increased to the level of the TMCS vapor methylated Si wafer substrate (θ_w = 74°) with approximately the same physical roughness and degree of hysteresis as that of dehydroxylated surfaces, bubble formation occurs. This evidence is important for two reasons. In the first instance, it demonstrates that the degree of hydrophobicity is important for bubble formation. This agrees with early theoretical analyses, which showed that quite apart from the geometry and size of surface sites hydrophobicity is essential for bubble formation on solid surfaces.[11] Second, considering that the physical roughness or "defects" are also only of nanoscale size (see Figure 7b), the observation of bubble formation on such smooth hydrophobic surfaces suggests that small defects in the nanometer range are large enough to act as physical sites for bubble growth on solid surfaces. There was no detectable bubble formation in the bulk solution and thus sites on the solid surface favor bubble formation. The small degree of hysteresis evident for these vapor-treated silicon wafers is sufficient to pin the three-phase contact line at the surface heterogeneity.

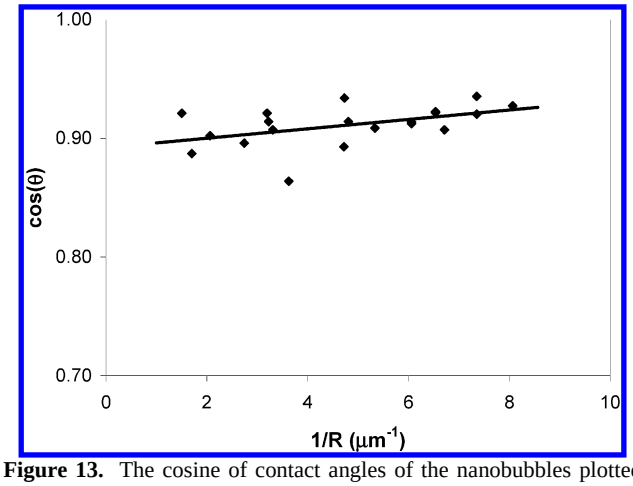

Figure 13. The cosine of contact angles of the nanobubbles plotted against the corresponding local curvatures based on the nanobubble images by TMAFM. The value of line tension calculated from the slope is approximately -3×10^{-10} N.

There are distinct differences in bubble size and distribution observed for bubble images obtained for the TMCS vapor treated surface and the TMCS in cyclohexane solution prepared surface (see Figures 7 and 9). The differences in bubble formation are due to the differences in surface roughness and hysteresis of the two kinds of substrates. The TMCS/cyclohexane-treated surface has a much higher surface roughness and larger hysteresis (see Table 1) compared with the TMCS vapor treated surfaces. We speculate that there may well be a larger number of surface sites on the former surface that stimulate bubble formation, perhaps leading to bubble growth and coalescence between adjacent, closely spaced sites. At this point we cannot identify these sites or their distribution with any more certainty.

Contact Angles and Line Tension. The water contact angles (or air contact angles) of the small bubbles on the methylated substrate surfaces (Figures 7−9) are much greater (smaller) than the contact angles measured by the sessile drop methods (Table 1). The contact angles of the small bubbles in Figures 7−9 can be determined from the cross section profile of each bubble. This may be extracted from the data file of a bubble examined by TMAFM (such as the one presented in Figure 11). For Figure 7, the advancing air contact angles of bubbles were found statistically to lie in the range from 23° to 30°. Similar observations were made by Ishida et al.[19] in their study. The radius of curvature of the AFM tips used falls between 5 and 20 nm. Following detailed work reported elsewhere on fluid droplets,[44,46] our very small bubble images are not distorted under our experimental conditions.

The difference between these macroscopic and microscopic contact angles may be linked to the influence of line tension.[44,45] The Young angle is modified by a line tension term when the droplet or bubble size is small,

$$\cos\theta = \cos\theta_{\mathrm{Y}} - \frac{\tau}{\gamma_{\mathrm{lv}} R} \qquad (1)$$

where θ is the actual contact angle that the very small bubble forms with the substrate, θ_{Y} is the Young contact angle, γ_{lv} is the liquid−vapor surface tension, $1/R$ is the local curvature of the bubble base on solid surface, and τ is the line tension. It should be pointed out that eq 1 reflects only line tension effects but does not consider the surface roughness and texture effects on the actual macroscopic or microscopic contact angle.[46,47,50]

Using eq 1, and examining some tens of bubbles, we show the dependence of local microscopic advancing air contact angles on the corresponding curvatures of the very small bubbles (examined from above) in Figure 13. The line tension of the bubbles, calculated from the gradient of the regression line, is -3×10^{-10} N. This value is similar in magnitude to the reported values of line tension for small droplets,[44,45] very close to the values determined by Scheludko et al.[51] and within the range anticipated theoretically.[52] The negative line tension of the three phase contact line acts to flatten the bubbles, reducing the Laplace pressure and thus stabilizing the very small bubbles formed at these solid−water interfaces.[48] We note that the large bubble contact angle is not recovered as R goes to infinity in Figure 13, behavior noticed elsewhere.[44,45] We cannot be certain as to the reason at this juncture but suspect that it may reflect differences in local surface texture for small bubbles compared with large ones[50] with, perhaps, additional mechanisms contributing as well.

Conclusion

The formation of very small gas bubbles (so-called "nanobubbles") at structured solid−water interfaces has been studied using the tapping mode atomic force microscopy (TMAFM) imaging technique. Silicon oxide wafer surfaces were prepared with different degrees of nanometer scale surface roughness and hydrophobicity. Small bubbles do not form on smooth, hydrophilic, or dehydroxylated silicon oxide wafer surfaces immersed in aqueous solutions under known levels of gas supersaturation. Randomly distributed small bubbles were observed over the whole surface of observation on methylated surfaces of controlled roughness. Bubbles formed on rough, methylated surfaces were larger and less-densely distributed than those on a smooth surface of similar hydrophobicity. The existence of these very small gas bubbles on the surface was further demonstrated by the observation of bubble coalescence with time. The macroscopic contact angle, measured with respect to the aqueous or gas phase, is very different from the microscopic contact angle detected by TMAFM and may be due to the influence of line tension at the three-phase contact line. Surface heterogeneities act to pin the contact line. The line tension has a value of -3×10^{-10} N and acts to stabilize the small bubbles, flattening them and thereby reducing the Laplace pressure. This Laplace pressure ranges from several to upward of 10 atmospheres for the very small bubbles encountered in this study.

Acknowledgment. Jingwu Yang acknowledges financial support from the Australian International Postgraduate Research Scholarship scheme. Discussions with Nataliya Mishchuk are warmly acknowledged.

References and Notes

(1) Dai, Z.; Fornasiero, D.; Ralston, J. *J. Chem. Soc., Faraday Trans.* **1998**, *94*, 1983.
(2) Jones, S. F.; Evans, G. M.; Galvin, K. P. *Adv. Colloid Interface Sci.* **1999**, *80*, 27.
(3) Harvey, E. N.; Cooper, K. W.; Whiteley, A. H. *J. Am. Chem. Soc.* **1946**, *68*, 9.
(4) Hemmingsen, E. A. *Nature* **1977**, *267*, 141.
(5) Carr, M. W.; Hillman, A. R.; Lubetkin, S. D.; Swann, M. J. *J. Electroanal. Chem. Interfacial Electrochem.* **1989**, *267*, 313.
(6) Lubetkin, S.; Akhtar, M. *J. Colloid Interface Sci.* **1996**, *180*, 43.
(7) Ryan, W. L.; Hemmingsen, E. A. *J. Colloid Interface Sci.* **1998**, *197*, 101.
(8) Clark, H. B.; Strenge, P. S.; Westwater, J. W. *Chem. Eng. Prog. Symp. Ser. Heat Transfer* **1959**, *55*, 103.
(9) Ryan, W. L.; Hemmingsen, E. A. *J. Colloid Interface Sci.* **1993**, *157*, 312.
(10) Vinogradova, O. I.; Bunkin, N. F.; Churaev, N. V.; Kiseleva, O. A.; Lobeyev, A. V.; Ninham, B. W. *J. Colloid Interface Sci.* **1995**, *173*, 443.

(11) Bankoff, S. G. *AIChE J.* **1958**, *4*, 24.
(12) Dean, R. *J. Appl. Phys.* **1944**, *15*, 446.
(13) Dill, K. A. *Science* **1990**, *250*, 297.
(14) Sharp, K. A.; Nicholls, A.; Fine, R. F.; Honig, B. *Science* **1991**, *252*, 106.
(15) Blander, M.; Katz, J. L. *AIChE J.* **1975**, *21*, 833.
(16) Bunkin, N. F.; Bunkin, F. V. *Zh. Eksp. Teor. Fiz.* **1992**, *101*, 512.
(17) Bunkin, N. F.; Kiseleva, O. A.; Lobeyev, A. V.; Movchan, T. G.; Ninham, B. W.; Vinogradova, O. I. *Langmuir* **1997**, *13*, 3024.
(18) Lou, S.-T.; Ouyang, Z.-Q.; Zhang, Y.; Li, X.-J.; Hu, J.; Li, M.-Q.; Yang, F.-J. *J. Vac. Sci. Technol., B* **2000**, *18*, 2573.
(19) Ishida, N.; Inoue, T.; Miyahara, M.; Higashitani, K. *Langmuir* **2000**, *16*, 6377.
(20) (a) Tyrrell, J. W. G.; Attard, P. *Phys. Rev. Lett.* **2001**, *87*, 176104/1. (b) *Langmuir*, **2002**, *18*, 160.
(21) Gong, W.; Stearnes, J.; Fornasiero, D.; Hayes, R. A.; Ralston, J. *Phys. Chem. Chem. Phys.* **1999**, *1*, 2799.
(22) Mahnke, J.; Stearnes, J.; Hayes, R. A.; Fornasiero, D.; Ralston, J. *Phys. Chem. Chem. Phys.* **1999**, *1*, 2793.
(23) Parker, J. L.; Claesson, P. M.; Attard, P. *J. Phys. Chem.* **1994**, *98*, 8468.
(24) Carambassis, A.; Jonker, L. C.; Attard, P.; Rutland, M. W. *Phys. Rev. Lett.* **1998**, *80*, 5357.
(25) Considine, R. F.; Drummond, C. J. *Langmuir* **2000**, *16*, 631.
(26) Ishida, N.; Sakamoto, M.; Miyahara, M.; Higashitani, K. *Langmuir* **2000**, *16*, 5681.
(27) Considine, R. F.; Hayes, R. A.; Horn, R. G. *Langmuir* **1999**, *15*, 1657.
(28) Attard, P. *Langmuir* **1996**, *12*, 1693.
(29) Ljunggren, S.; Eriksson, J. C. *Colloids Surf., A* **1997**, *129*−*130*, 151.
(30) Fielden, M. L.; Hayes, R. A.; Ralston, J. *Langmuir* **1996**, *12*, 3721.
(31) Blake, P.; Ralston, J. *Colloids Surf.* **1985**, *15*, 101.
(32) Newcombe, G.; Ralston, J. *Langmuir* **1992**, *8*, 190.
(33) Babcock, K. L.; Prater, C. B. *Phase Imaging: Beyond Topography*; Digital Instruments Support Note; 1995.
(34) Beake, B. D.; Leggett, G. J.; Shipway, P. H. *Surf. Interface Anal.* **2001**, *31*, 39.
(35) Butler, J. N. *Carbon Dioxide Equilibria and Their Applications*; Addison-Wesley Publishing Company, Inc.: Reading, MA, 1982.
(36) Jacobs, K. Personal communication.
(37) Biggs, S.; Grieser, F. *J. Colloid Interface Sci.* **1994**, *165*, 425.
(38) Tripp, C. P.; Hair, M. L. *Langmuir* **1992**, *8*, 1961.
(39) Trau, M.; Murray, B. S.; Grant, K.; Grieser, F. *J. Colloid Interface Sci.* **1992**, *148*, 182.
(40) Chen, G. Y.; Warmack, R. J.; Oden, P. I.; Thundat, T. *J. Vac. Sci. Technol., B* **1996**, *14*, 1313.
(41) Everett, D. H. *Basic Principles of Colloid Science*; The Royal Scoiety of Chemistry: London, 1988.
(42) Mullin, J. W. *Crystallization*, 3 ed.; Butterworth-Heinemann Ltd, Printed by Ipswich Book Co. Ltd: Ipswich, Suffolk, Great Britain, 1993.
(43) Hemmingsen, E. A. *J. Appl. Phys.* **1975**, *46*, 213.
(44) Pompe, T.; Herminghaus, S. *Phys. Rev. Lett.* **2000**, *85*, 1930.
(45) Herminghaus, S.; Fery, A.; Schlagowski, S.; Jacobs, K.; Seemann, R.; Gau, H.; Monch, W.; Pompe, T. *J. Phys.: Condens. Matter* **1999**, *11*, A57.
(46) Wenzel, R. N. *J. Phys. Colloid Chem.* **1949**, *53*, 1466.
(47) Drelich, J.; Miller, J. D.; Good, R. J. *J. Colloid Interface Sci.* **1996**, *179*, 37.
(48) Boehnkea, U. C.; Remmlera, T.; Motschmannb, H.; Wurlitzera, S.; Hauwedea, J.; Fischera, T. M. *J. Colloid Interface Sci.* **1999**, *211*, 243.
(49) Vansant, E. F., van der Woort, P.; Vrancken, K. C. *Characterization and Chemical Modification of the Silica Surface*; Elsevier: Amsterdam, 1995.
(50) Huh, C.; Mason, S. G. *J. Colloid Interface Sci.* **1977**, *60*, 11.
(51) Scheludko, A.; Toshev, B.; Bogadiev, B. *J. Chem. Soc., Faraday Trans.* **1976**, *72*, 2815.
(52) Buff, F. P.; Saltsburg, H. T. *J. Phys. Chem.* **1957**, *26*, 23.
(53) Snoswell, D.; Duan, J.; Fornasiero, D.; Ralston, J. *J. Phys. Chem. B* **2003**, *107*, 2986.